

Rising atmospheric methane: 2007-14 growth and isotopic shift.

E.G. Nisbet¹, E.J. Dlugokencky², M.R. Manning³, D. Lowry¹, R.E. Fisher¹, J.L. France^{1,4}, S. E. Michel⁵, J.B. Miller^{5,6}, J.W.C. White⁵, B. Vaughn⁵, P. Bousquet⁷, J.A. Pyle⁸, N.J. Warwick⁸, M. Cain⁸, R. Brownlow¹, G. Zazzeri¹, M. Lanoisellé¹, A.C. Manning⁴, E. Gloor⁹, D.E.J. Worthy¹⁰, E.-G. Brunke¹¹, C. Labuschagne^{11,12}, E.W. Wolff¹³, A.L. Ganesan¹⁴

1. Dept. of Earth Sciences, Royal Holloway, Univ. of London, Egham TW20 0EX, United Kingdom.
2. US National Oceanic and Atmospheric Administration, Earth System Research Laboratory, 325 Broadway, Boulder, CO 80305, USA.
3. Climate Change Research Institute, School of Geography Environment and Earth Sciences, Victoria University of Wellington, New Zealand.
4. Centre for Ocean and Atmospheric Sciences, School of Environmental Sciences, University of East Anglia, Norwich NR4 7TJ, United Kingdom.
5. Institute of Arctic and Alpine Research, University of Colorado, Boulder CO, USA.
6. Cooperative Institute for Research in Environmental Sciences, University of Colorado, Boulder, CO 80305, USA.
7. Laboratoire des Sciences du Climat et de l'Environnement, 91191 Gif-sur-Yvette Cedex, France.
8. Department of Chemistry, University of Cambridge, Lensfield Road, Cambridge, CB2 1EW, and National Centre for Atmospheric Science (NCAS), United Kingdom.
9. School of Geography, University of Leeds, Leeds, United Kingdom.
10. Environment Canada, 4905 Dufferin St., Downsview, Ontario, M3H 5T4 Canada.
11. South African Weather Service, P.O. Box 320, Stellenbosch 7599, South Africa.
12. School of Physical and Chemical Sciences, North-West University, Potchefstroom, South Africa.
13. Department of Earth Sciences, University of Cambridge, Downing St., Cambridge, CB2 3EQ, United Kingdom.
14. School of Geographical Sciences, University of Bristol, University Rd, Bristol BS8 1SS, United Kingdom.

Corresponding author: Euan G. Nisbet (e.nisbet@rhul.ac.uk)

Key Points:

- Atmospheric methane has risen sharply since 2007, increasing by 12.5 ± 0.4 ppb in 2014.
- Concurrently there has been an isotopic shift to more negative stable carbon isotope ratios.
- The likely cause is increased biogenic emissions in the tropics and Southern Hemisphere.

39 Abstract

40 From 2007 to 2013, the globally-averaged mole fraction of methane in the atmosphere increased
41 by 5.7 ± 1.2 ppb yr^{-1} . Simultaneously, $\delta^{13}\text{C}_{\text{CH}_4}$ (a measure of the $^{13}\text{C}/^{12}\text{C}$ isotope ratio in methane)
42 has shifted to significantly more negative values since 2007. Growth was extreme in 2014, at
43 12.5 ± 0.4 ppb, with a further shift to more negative values being observed at most latitudes. The
44 isotopic evidence presented here suggests the methane rise was dominated by significant
45 increases in biogenic methane emissions, particularly in the tropics: for example, from expansion
46 of tropical wetlands in years with strongly positive rainfall anomalies, or emissions from
47 increased agricultural sources such as ruminants and rice paddies. Changes in the removal rate of
48 methane by the OH radical have not been seen in other tracers of atmospheric chemistry and do
49 not appear to explain short term variations in methane. Fossil fuel emissions may also have
50 grown, but the sustained shift to more ^{13}C -depleted values together with its significant
51 interannual variability, and the tropical and Southern Hemisphere loci of post-2007 growth, both
52 indicate fossil fuel emissions have not been the dominant factor driving the increase. A major
53 cause of increased tropical wetland and tropical agricultural methane emissions, the likely major
54 contributors to growth, may be their responses to meteorological change.

55 1 Introduction

56 The methane content of the atmosphere began rising again in 2007 after a growth slow-down that
57 had first become apparent in the late 1990s (Dlugokencky et al., 1998, Nisbet et al., 2014). The
58 mole fraction of Southern Hemisphere atmospheric methane varied little for seven years up to
59 2006, but then started to increase in early 2007. Since 2007, sustained increases in atmospheric
60 methane mole fraction have occurred in most latitudinal zones of the planet, but with major local
61 short-term excursions from the overall spatial pattern of growth (Fig.1). In the Northern
62 Hemisphere autumn of 2007, rapid growth was measured in the Arctic and boreal zone (Fig. 1).
63 However, both in 2007 and thereafter, global growth has dominantly been driven by the latitudes
64 south of the Arctic/boreal zone, for example both north and south of the equator in 2008, and in
65 the southern tropics in 2010-11. Even compared to the increases of preceding years, 2014 was
66 exceptional, with extremely strong annual (1 January 2014 to 1 January 2015) growth at all
67 latitudes, especially in the equatorial belt (Fig. 1).

68
69 CH_4 mole fractions provide insufficient information to determine definitively the causes of the
70 recent rise (Kirschke et al., 2013). Isotopic measurements (Dlugokencky et al., 2011) provide
71 powerful constraints that can help to identify specific source contributions. Atmospheric methane
72 is also becoming more depleted in the isotope ^{13}C . At any individual location, local
73 meteorological factors such as shifting prevailing wind directions may influence measurements:
74 however, the sustained nature of the increase and isotopic shift, and the regional and global
75 distribution of the methane growth, imply that major ongoing changes in methane budgets are
76 occurring.

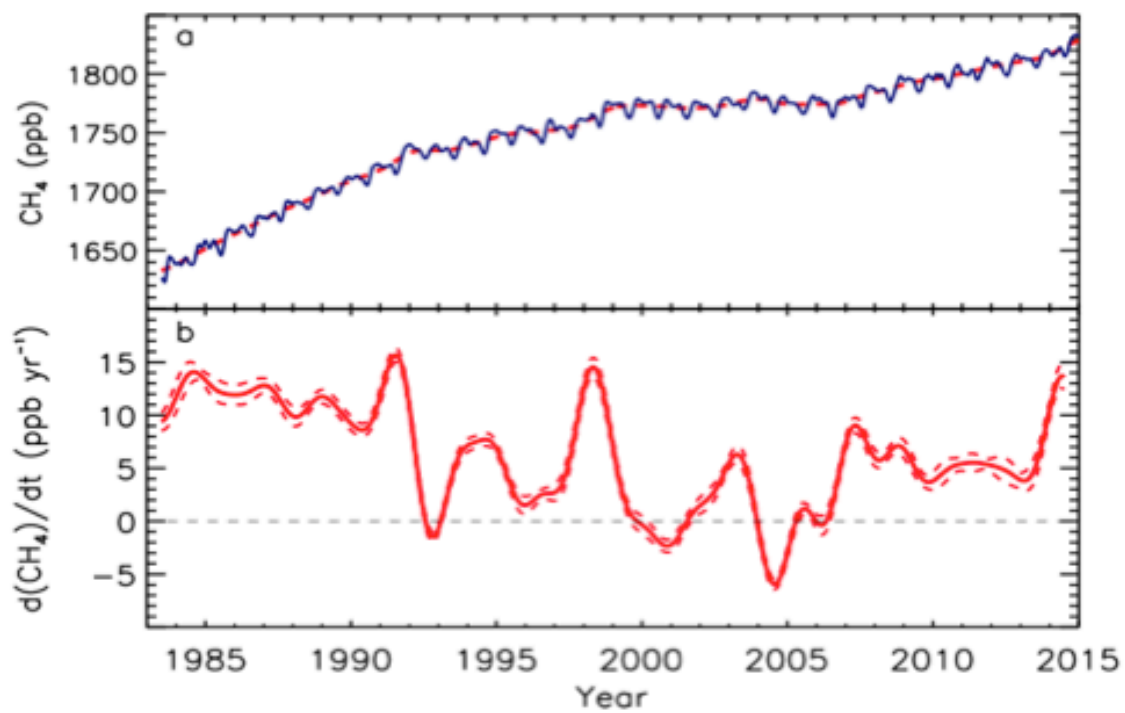
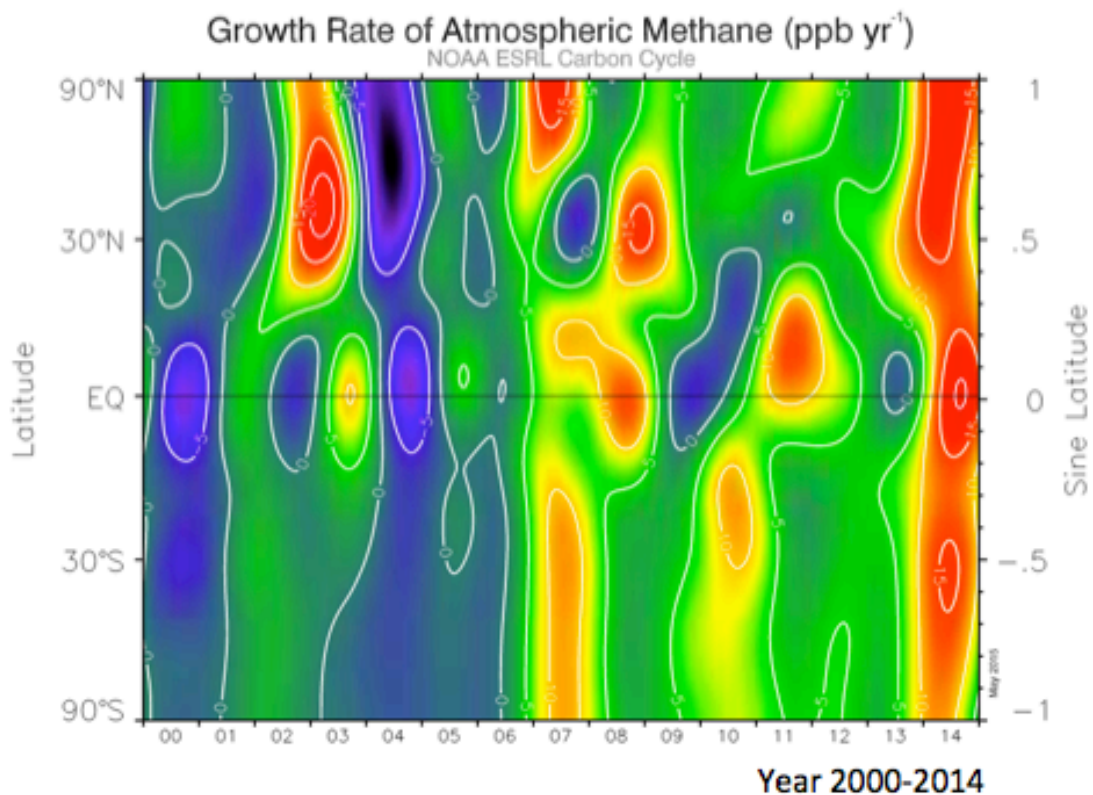
77
78 Recently, Schaefer et al. (2016) used a one-box model of CH_4 mole fraction and $\delta^{13}\text{C}_{\text{CH}_4}$ isotopic
79 data to reconstruct the global history of CH_4 emissions to the atmosphere. They concluded that
80 the isotopic evidence demonstrates that emissions of thermogenic methane (e.g. from fossil fuels
81 and biomass burning) were not the dominant cause of the post-2007 growth, and pointed out that
82 this contradicts emission inventories. In contrast, Schaefer et al. (2016) concluded that the cause
83 of the post-2007 rise was primarily an increase in biogenic emissions and that these emissions

84 were located outside the Arctic. Furthermore, they inferred that the increased emissions were
85 probably more from agricultural sources than from wetlands.

86
87 The evidence reported here includes new Atlantic and Arctic methane mole fraction and isotopic
88 data, and develops the analysis by using a running budget analysis (see SI Section 16) of
89 monthly averages over four latitude zones instead of annual averages and a one-box model. This
90 detailed analysis permits latitudinal differentiation of changes in CH₄ emission sources, which
91 our isotopic data show have significant interannual variability in the overall trend to more
92 negative values since 2007.

93
94 Fig.1 illustrates the CH₄ record over the three decades since the start of detailed global
95 monitoring by NOAA (http://www.esrl.noaa.gov/gmd/ccgg/trends_ch4/). The very high growth
96 rates in the 1980s (~14 ppb in 1984, and >10 ppb yr⁻¹ though 1983-91) (Dlugokencky et al.,
97 1998; Dlugokencky et al., 2011) were driven by the strong increase in anthropogenic emissions
98 in the post-War years, for example from the Soviet gas industry (Dlugokencky et al., 1998). In
99 1992 the eruption of Mt. Pinatubo and the major *El Niño* event had important impacts on sources
100 and sinks. Following this, growth rates declined. Major reductions in leaks from the gas industry
101 may have contributed to the reduction in growth rates (Dlugokencky et al., 1998). Strong growth
102 resumed briefly during the strong *El Niño* event of 1997-8, but apart from this single event,
103 methane growth rates were subdued in the period 1992-2007. The overall trend from 1983-2007
104 is consistent with an approach to equilibrium (Dlugokencky et al., 2011), implying no trend in
105 total global emissions and an atmospheric lifetime of approximately 9 years.

106
107 Fig. 1. Global trends in CH₄ from 2000 to the end of 2014.
108 Top panel: Global sine-latitude vs time plot of CH₄ growth rate. Green, yellow and red colors
109 show increases, blue, dark blue, and violet show declines, contoured in increments of 5 ppb yr⁻¹.
110 Lower panel: Globally averaged methane, and growth rates 1983-2014. a) – atmospheric mole
111 fraction. Red dashed line is a deseasonalized trend curve fitted to the global averages. b) –
112 instantaneous growth rate from the time-derivative of the red dashed line in the top panel. Thin
113 dashed lines are $\pm 1\sigma$.



115 2 Methods

116 Observations reported here are from measurements made by the USA National Oceanic and
117 Atmospheric Administration (NOAA) Cooperative Global Air Sampling Network, for whom the
118 Institute of Arctic and Alpine Research (INSTAAR) carry out $\delta^{13}\text{C}_{\text{CH}_4}$ measurement on a subset
119 of the same air samples analyzed for CH_4 , by Royal Holloway, University of London (RHUL,
120 UK) and by the University of Heidelberg (UHEI). Details are given in the Supporting
121 Information sections 6, 7, and 8. Mole fraction measurements are reported on the WMO X2004A
122 scale (Dlugokencky et al., 2005 updated at: http://www.esrl.noaa.gov/gmd/ccl/ch4_scale.html).
123 By comparing data from different laboratories, we have checked for systematic bias among the
124 measurement programs. Further details on RHUL-INSTAAR inter-comparison are in the
125 Supporting Information sections 8, 9 and 10.

126 3 Measurements

127 To understand the factors driving global methane trends in the past decade, we focus on key
128 background stations in regions where significant methane events have occurred: 1) the Arctic
129 and boreal zone; 2) the Atlantic Equatorial Tropics; and 3) the Southern Hemisphere.

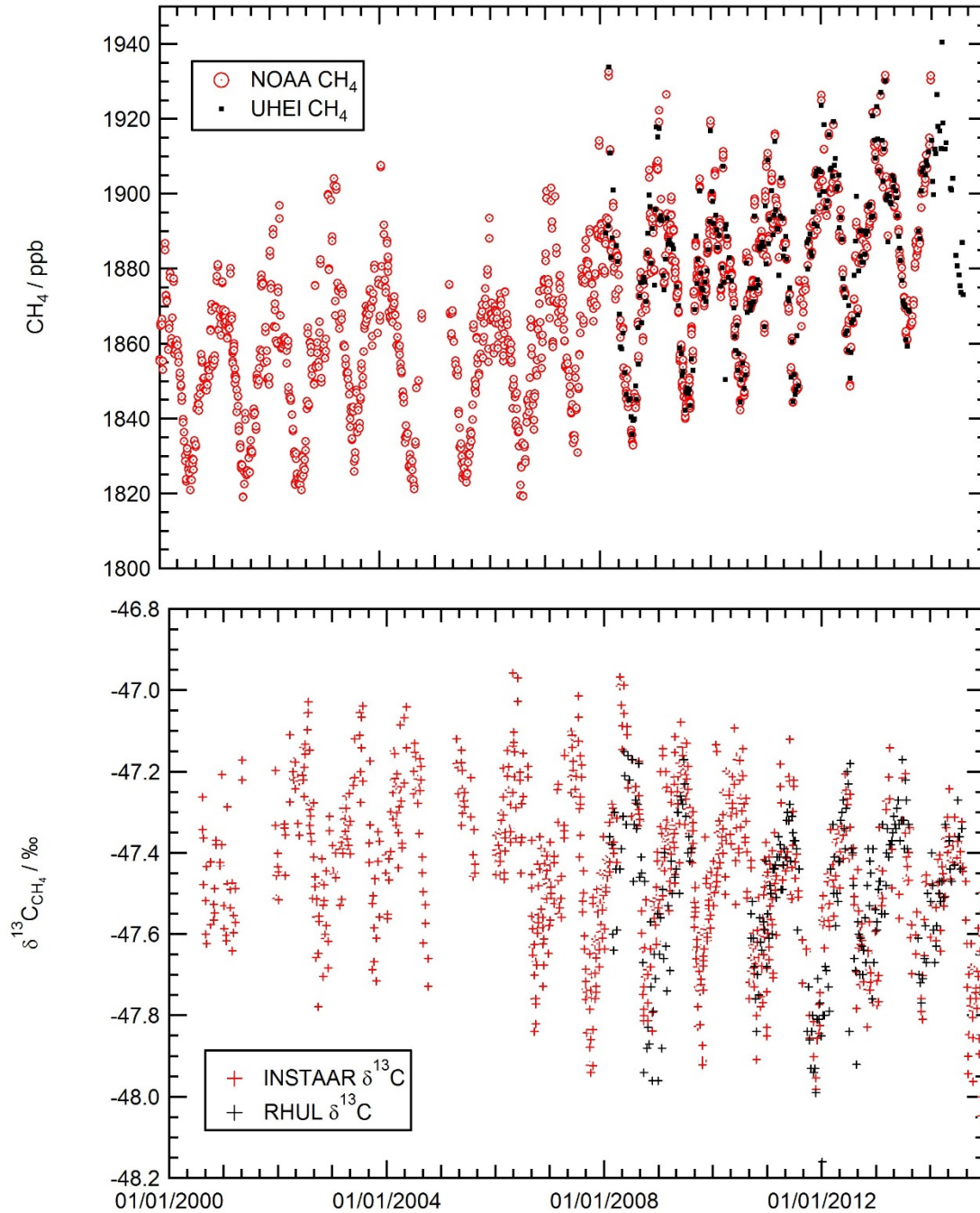
130
131 From 2007 to 2013, we report that the globally-averaged mole fraction of methane in the
132 atmosphere increased by 5.7 ± 1.2 ppb yr^{-1} (parts per billion, or nmole mol^{-1} , dry air, ± 1 standard
133 deviation of annual increases; uncertainty of each annual increase is $\sim \pm 0.5$ ppb yr^{-1}). Growth has
134 continued strongly with an increase of 12.5 ± 0.4 ppb in 2014. Simultaneously, results presented
135 here show $\delta^{13}\text{C}_{\text{CH}_4}$ (a measure of the $^{13}\text{C}/^{12}\text{C}$ isotope ratio in methane) has recently shifted
136 significantly to more negative values. For example, prior to 2007, as monitored in remote
137 equatorial Southern Hemisphere air at Ascension Island, $\delta^{13}\text{C}_{\text{CH}_4}$ was stable or increased slightly,
138 with $\delta^{13}\text{C}_{\text{CH}_4}$ changing by less than $+0.01\text{‰ yr}^{-1}$. Post 2007, $\delta^{13}\text{C}_{\text{CH}_4}$ started to decrease. The shift
139 has been in excess of -0.03‰ yr^{-1} , with a total shift of $0.24 \pm 0.02\text{‰}$ by 2014. Similar patterns to
140 those observed at Ascension have been observed globally, though with regional variation (Fig. SI
141 10).

142 143 3.1 Methane $\delta^{13}\text{C}_{\text{CH}_4}$ in high Northern latitudes: Alert, Canada ($82^{\circ}27'\text{N}$, $62^{\circ}31'\text{W}$)

144
145 Methane mole fractions (Fig. 2 upper panel and Fig. SI 1) in NOAA air samples from Alert,
146 Nunavut, Canada, which are representative of the western Arctic, show a sharp increase in
147 summer 2007. In September 2007, methane measured at Alert was 16 ppb higher than in the
148 previous September, although note that single month comparisons can depend heavily on
149 sustained local meteorological conditions. That year, the annual increase averaged over 53°N to
150 90°N was 13.3 ± 1.3 ppb. But this was not sustained. In 2008, 2010 and markedly so in 2011-12,
151 Arctic growth was below global means. As fast horizontal mixing at high latitudes efficiently
152 links Arctic emission zones with Alert (Bousquet et al., 2011), this indicates that from 2008-2013
153 no major sustained new methane emission increase occurred in the wider Arctic. In 2014, year-
154 on-year strong Arctic increases began anew (Fig. SI 1), but at a rate comparable with the global
155 increase that year.

156
157 In the NOAA air samples from Alert, an overall isotopic trend to more depleted $\delta^{13}\text{C}_{\text{CH}_4}$ is
158 apparent, beginning in about 2006 (Fig. 2 lower panel). Since 2008, $\delta^{13}\text{C}_{\text{CH}_4}$ measurements made

159 by RHUL and NOAA on Alert air samples show that this overall negative trend has been
 160 maintained through 2013, with a slight positive relaxation since (Fig. 2 lower panel and Fig. SI
 161 10).
 162



163
 164 Figure 2.

165 Methane mole fraction (upper panel) and $\delta^{13}\text{C}_{\text{CH}_4}$ isotope measurements (lower panel) in discrete
166 air samples collected from Alert, Canada. Mole fraction data from NOAA and Univ. of
167 Heidelberg (UHEI) samples; isotopic measurements from NOAA-INSTAAR and RHUL.

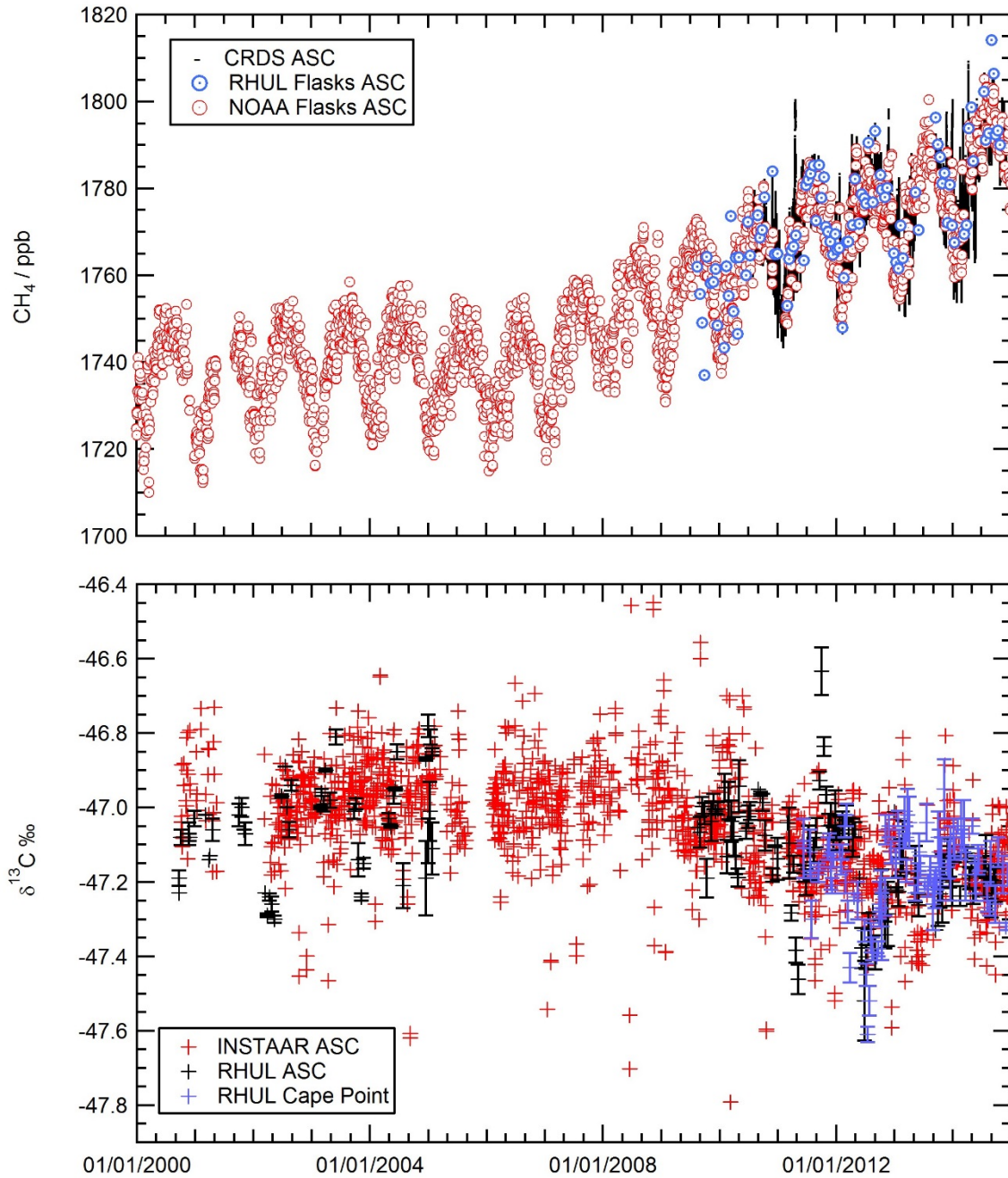
169 **3.2 Atlantic Equatorial air – Methane and $\delta^{13}\text{C}_{\text{CH}_4}$ at Ascension Island (7°58'S, 14°24'W)**

170 At Ascension Island, strong growth in methane has been sustained from 2007-2014 (Fig. 3 upper
171 panel; see also Figs. SI 3 & 4). Taking all RHUL and NOAA measurements together, in 2010-
172 2011 year-on-year (January to January) growth, calculated from a smoothed spline, was 10.1 ± 2.9
173 ppb, in contrast to the global growth rate of 5.0 ± 0.7 ppb in the NOAA data that year. In 2011-
174 12, an HPspline curve fit (Pickers and Manning 2015) of the Ascension record shows moderate
175 growth compared to other years (3.4 ± 1.1 ppb), and again in 2012-13 (3.0 ± 0.9 ppb) followed by
176 stronger growth in 2013-14 (8.9 ± 2.7 ppb, compared to a global growth of 5.9 ± 0.5 ppb).
177 Following 2014, very strong growth has resumed, with the year-on-year growth in monthly
178 averages well over 10 ppb yr^{-1} . In 2014-15, RHUL measurements show extreme growth of
179 12.7 ± 2.3 ppb, especially towards the end of the year (but note that at a single location, short
180 timescale meteorological variability can have large impact on year-on-year comparison). Further
181 details of growth are given in the Supporting Information section 4 and Fig. SI 3.

182
183 In low latitudes of the Southern Hemisphere, between the equator and 30°S (i.e. southern tropics
184 and extratropical winter rainfall belts), smoothed annual (January to January) growth trends in
185 the NOAA network show similar behavior. In this latitudinal zone there was near-zero growth
186 from 2001-2006 (including a decline in 2004 and 2005) followed by growth of 7.9 ± 0.5 ppb in
187 2007; 7.0 ± 0.5 ppb in 2008, 2.6 ± 0.5 ppb in 2009, 8.1 ± 0.4 ppb in 2010, 4.8 ± 0.3 ppb in 2011,
188 4.3 ± 0.3 ppb in 2012, 5.8 ± 0.5 ppb in 2013, and 11.2 ± 0.4 ppb in 2014.

189
190 The $\delta^{13}\text{C}_{\text{CH}_4}$ record of marine boundary air sampled at Ascension Island is shown in Fig. 3
191 (lower panel). In general, methane in the Southern Hemisphere, much of which has passed
192 through the OH-rich region in the mid-troposphere around the brightly-lit and humid
193 Intertropical Convergence Zone (ITCZ), is slightly 'heavier', that is, richer in ^{13}C , than north of
194 the equator, where the dominant sources are located. Error bars in individual measurements are
195 also shown in the figure. The data show poorly defined $\delta^{13}\text{C}_{\text{CH}_4}$ isotopic seasonality, and from
196 2001-2005 show no significant trend. Both NOAA and RHUL datasets independently show a
197 shift ($>0.2\text{‰}$) to more ^{13}C -depleted values from 2009, becoming more marked with excursions to
198 much more negative values in early 2011 and 2012. Values have since recovered to slightly less
199 negative values by the end of 2014 but Ascension $\delta^{13}\text{C}_{\text{CH}_4}$ values through into 2015 have
200 stabilized around 0.2‰ more negative than in 2007-8. This shift is far greater than experimental
201 uncertainty (see error bars on figure). If the trends are assumed to be linear, the shift pre-2007
202 was less than $+0.01\text{‰ yr}^{-1}$; post 2007, the shift has been in excess of -0.03‰ yr^{-1} (see Fig. SI 4).
203 Ongoing 2015 $\delta^{13}\text{C}_{\text{CH}_4}$ measurements suggest continuing decline. The assumption of a linear
204 change in $\delta^{13}\text{C}_{\text{CH}_4}$ is however a broad simplification.

205



206

207 Figure 3

208 Upper panel. Methane mole fraction from Airhead, Ascension Island. Red circles are NOAA
 209 discrete air samples from 2000. The black line shows RHUL continuous observations and blue
 210 squares show RHUL flask air samples from the same site.

211 Lower panel. South Atlantic $\delta^{13}\text{C}_{\text{CH}_4}$ data, 2000-2015. The graph shows both NOAA-INSTAAR
 212 (red crosses) and RHUL measurements (black crosses, showing error bars) from Ascension
 213 (ASC) and RHUL data from Cape Point, South Africa (CPT; purple crosses and error bars). See

214 Fig. SI 4 for trend analysis: Change in $\delta^{13}\text{C}_{\text{CH}_4}$ pre-2007 was less than $+0.01\text{‰ yr}^{-1}$; post 2007,
 215 the shift has been in excess of -0.03‰ yr^{-1} .

216
 217 **3.3 Comparison with other southern latitude sites: Cape Point, South Africa (34°21'S,**
 218 **18°30'E), and South Pole**

219
 220 Hybrid Single Particle Lagrangian Integrated Trajectory model (HYSPPLIT)
 221 (http://www.arl.noaa.gov/HYSPLIT_info.php) (Stein et al. 2015) air mass backward trajectories
 222 indicate that much of the air reaching Ascension in early to mid-2012 was from the south-
 223 western South Atlantic, including prior inputs of air from south of the equator in South America
 224 (see Fig. SI 2), and from the Southern Ocean. From Cape Point, the RHUL flask sampling record
 225 of methane mole fraction and $\delta^{13}\text{C}_{\text{CH}_4}$ (Fig 3; see also Fig. SI5) begins in 2011, and the NOAA
 226 record in 2009. There was moderate annual growth in mole fraction (5 ppb in 2011-12, 3 ppb in
 227 2012-13) until 2013-14, when a strong (>10 ppb) year-on-year rise took place. The RHUL
 228 $\delta^{13}\text{C}_{\text{CH}_4}$ record shows a sharp shift to isotopically more negative values in 2012, reverting to
 229 previous levels in early 2013 and then perhaps becoming slightly more negative again in 2014.
 230 These Cape Point values are similar to those observed in RHUL air samples from Ascension
 231 over the same time.

232
 233 Southern Hemisphere background trends are represented by NOAA samples from the South Pole
 234 (Figs. SI6 & 7). These measurements record strong and sustained methane growth from 2007
 235 onwards. In the polar Southern Hemisphere, (60-90°S), zonal average annual means were
 236 1726 ± 0.1 ppb in 2006, rising to 1774 ± 0.1 ppb in 2014. Concurrent with this growth is a
 237 sustained shift to more negative $\delta^{13}\text{C}_{\text{CH}_4}$, also beginning around 2006 (see Figs. SI 6, 8). The
 238 pronounced negative dip observed at the South Pole in late 2011 is comparable to the Ascension
 239 dip in 2011 and 2012. At the South Pole, as for Ascension, if the $\delta^{13}\text{C}_{\text{CH}_4}$ trends are assumed to
 240 be linear, the shift pre-2007 was negligible; post-2007, the shift has been about -0.03‰ yr^{-1} (See
 241 Fig. SI 8).

242
 243 **4 Global evolution of trends in methane mole fraction and isotopic values**

244
 245 What hypotheses can be proposed to account for these observations? In this section, possible
 246 explanations are proposed, both for the Arctic trends, and for the trends observed in the savanna
 247 and equatorial tropics, then in Section 5 a running budget analysis is used to investigate the
 248 hypotheses for plausibility in matching the mole fraction and isotopic records.

249
 250 **4.1 Possible explanations of the observed growth and isotopic shift, Arctic and Tropical**
 251 **zones.**

252
 253 Bousquet et al. (2006) found that declining growth rates in anthropogenic emissions were the
 254 cause of the decreasing atmospheric methane growth rates during the 1990s, but that after 1999
 255 anthropogenic emissions of methane rose again. The effect of this increase was initially masked
 256 by a decrease in wetland emissions, but remote sensing data show that surface water extent
 257 started to increase again in 2002 (Prigent et al., 2012). Recent widening of the Hadley Cell (Min
 258 and Son, 2013; Tselioudis et al, 2016) would have extended the high rainfall zone under the

259 ITCZ, increasing both natural wetland and agricultural emissions in the tropics. Thus these
 260 sources are discussed in detail, by region.

261
 262 ***Arctic***
 263 The most obvious explanation of the increase in Arctic methane in 2007 is an increase in
 264 emissions. If so, isotopic and time-of-season constraints both point to increased late summer
 265 Arctic and boreal wetland emissions. Methane emitted from Arctic and boreal wetlands is
 266 markedly depleted isotopically: in Fennoscandia, atmospheric sampling and Keeling plot studies
 267 (Fisher et al., 2011; Sriskantharajah et al., 2012) showed the emissions had $\delta^{13}\text{C}_{\text{CH}_4}$ values of -
 268 $70\pm 5\%$, while Canadian boreal wetland emissions are around $-67\pm 2\%$ (unpublished RHUL
 269 studies). These values are close to the $\delta^{13}\text{C}_{\text{CH}_4}$ value of around -68% of the regional Arctic
 270 summer methane increment over Atlantic background, indicating the summer source is mainly
 271 from wetlands (Sriskantharajah et al., 2012; Fisher et al., 2011). In contrast, gas field and hydrate
 272 sources are too enriched in ^{13}C to produce the observed shift. Siberian gas fields are very large,
 273 but typically have $\delta^{13}\text{C}_{\text{CH}_4}$ around $-50\pm 3\%$ (Dlugokencky et al., 2011), which is close to bulk
 274 atmospheric values and after dilution in regional air masses would be unlikely to produce the
 275 shift observed in the Alert values. Similarly, Fisher et al. (2011) and Berchet et al. (2016) found
 276 no evidence for large hydrate emissions.

277
 278 Thus, the most likely explanation of the sharp growth in Arctic methane in late 2007, and the
 279 concurrent trend to more negative $\delta^{13}\text{C}_{\text{CH}_4}$ values in ambient Arctic methane, is an increase in
 280 wetland emissions. 2007 was an exceptional year in the Arctic, when the North American Arctic
 281 wetlands experienced unusually sunny skies and large temperature increases compared to past
 282 records, with warm southerly winds (Kay et al., 2007). The anomalous temperatures and
 283 southerly winds (Comiso et al., 2008) likely drove very strong growth of summer and autumn
 284 emissions from Arctic and boreal wetlands. Bergamaschi et al. (2013) reported an increase in
 285 emissions of 2-3 Tg CH_4 in 2007, then below average emissions from 2008-2010. Similarly,
 286 Bruhwiler et al. (2014) estimated that in 2007, the emissions were 4.4 Tg CH_4 higher than the
 287 decadal average. The very depleted $\delta^{13}\text{C}_{\text{CH}_4}$ values from Alert in autumn 2007 thus most
 288 probably record the presence of methane-rich boreal and Arctic wetland air.

289
 290 From 2008-2013, growth of methane and isotopic shifts in the Arctic were unexceptional
 291 compared to the global record; in 2014 very strong growth occurred, but similar growth occurred
 292 elsewhere worldwide. Overall, although Arctic emissions contributed to the Arctic methane shift
 293 in 2007, they do not seem to have been major contributors since then.

294
 295 ***Tropics and Southern Hemisphere: Isotopic signatures of sources south of 30°N***
 296 Most of the strongest growth in methane since 2007 has been led by the wider Tropics, here
 297 taken as the zone between the Tropics of Cancer and Capricorn ($23^{\circ}26'$), and also including the
 298 region experiencing passage of the Inter-Tropical Convergence Zone (ITCZ) in South and East
 299 Asia. Bousquet et al (2016) found from top-down studies that almost two-thirds ($\sim 64\%$) of the
 300 global methane emissions are from south of 30°N , while latitudes north of 60°N contribute only
 301 4%. In the tropics, the main biogenic methane emissions are in sub-equatorial and savanna
 302 wetlands, from rice paddies and ruminants in southern and Southeast Asia, and from ruminants
 303 in India, South America and savanna Africa (Kirschke et al., 2013; Dlugokencky et al., 2011), on
 304 grasslands dominated by grasses using the C4 pathway, as well as widespread biomass burning,

305 especially in Africa's C4 savannas. The main anthropogenic sources in the region are not well
306 quantified but include large ruminant populations, especially in Indian but also in China,
307 Southeast Asia, South America and Africa, in addition to dry season (winter) biomass burning.
308 Thermogenic fossil fuel sources in the region include South Africa's coal industry, sub-
309 equatorial gas fields in South America, and widespread large gas fields and coal fields in Asia
310 and Australia.

311
312 $\delta^{13}\text{C}_{\text{CH}_4}$ values of tropical wetland methane emissions to the air (as opposed to methane within
313 the water/vegetation/mud columns) are poorly constrained but appear typically to be around -
314 $54\pm 5\%$ (unpublished RHUL results in Uganda, Southeast Asia, Peru, Ascension; and from
315 Dlugokencky et al., 2011). This contrasts with values of around -68% for Arctic wetlands
316 (Fisher et al., 2011). In the northern tropics, wetland flooding from run-off is typically in the late
317 rainy season (August-September onwards) or later in river-fed swamps. Conversely, in the
318 southern tropics (e.g. Bolivia, Zambia) wetlands fill in February-March onwards. Tropical
319 seasonal wetland emissions are readily distinguishable from dry season biomass burning
320 emissions that come a few months later from the same general regions. Methane in smoke from
321 grass fires in tropical C4 grasslands in winter (NH: Nov-Feb; SH: May-Aug) has $\delta^{13}\text{C}_{\text{CH}_4}$ values
322 around -20% to -10% (unpublished RHUL results and see SI section 1 and Dlugokencky et al.,
323 2011). Thus biomass burning injects methane with $\delta^{13}\text{C}_{\text{CH}_4}$ that is more positive than the
324 atmosphere: in this context, the continuing shift to negative values in 2014, an El Nino year, is of
325 interest as such events are usually associated with biomass burning (Duncan et al. 2003).

326
327 The $\delta^{13}\text{C}_{\text{CH}_4}$ values of tropical ruminant methane emissions have been very little studied in the
328 field. Schaefer et al. (2016) assumed ruminants are C3-fed and emit methane with $\delta^{13}\text{C}_{\text{CH}_4}$ of -
329 60% , but grasslands and ruminant fodder crops in the tropics tend to be C4 rather than C3
330 dominated. Dlugokencky et al. (2011) considered C4 ruminant methane emissions to be $-49\pm 4\%$
331 and thus tropical ruminant emissions are likely more enriched in $\delta^{13}\text{C}_{\text{CH}_4}$ than the 60% value
332 assumed by Schaefer et al. (2016). Many free-grazing tropical ruminants live in C4 savanna
333 grasslands, and supplemental fodder may be maize, millet, or sorghum crop waste, or sugar cane
334 tops, all $\delta^{13}\text{C}_{\text{CH}_4}$ -enriched C4 plants. Thus it is likely that methane from such cows is
335 substantially more enriched than the -60% C3 value, and more likely to have $\delta^{13}\text{C}_{\text{CH}_4}$ values
336 around -50% or less (Dlugokencky et al., 2011). But tropical data are very sparse.

337
338 Fossil fuel emissions in the region south of 30°N are typically isotopically enriched in $\delta^{13}\text{C}_{\text{CH}_4}$,
339 although published isotopic measurements are few. For example, Bolivian gas in La Paz is -35%
340 (unpublished RHUL results), while the very large Pars gas field in Qatar/Iran is -40% (Galimov
341 and Rabbani, 2001). Methane from Chinese coal is also isotopically enriched and likely to be in
342 the -35 to -45% range (own observations and see Thompson et al., 2015). Southern Hemisphere
343 Gondwana coalfield methane from Australia is close to bulk atmospheric values (Hamilton et al.,
344 2014), but some mines can be isotopically depleted compared to the atmosphere (Zazzeri et al.,
345 2016). In the Hunter coalfield of Australia (typical of large coal mines in the Southern
346 Hemisphere), Zazzeri et al. (2016) report $\delta^{13}\text{C}_{\text{CH}_4}$ of $-66.4\pm 1.3\%$ from surveys around
347 bituminous coal mines, and -60.8 ± 0.3 around a ventilation shaft. Some of the more negative
348 values may reflect the input of secondary biogenic methane into the coalfield emissions.
349 Worldwide, open cast coal mining may be associated with the production of some isotopically
350 lighter microbial methane.

351
352 To summarise overall, although much better site-by-site information is needed, and while
353 emissions from a few fossil sources are isotopically relatively depleted compared to the
354 atmosphere, methane emissions from the majority of large gas and coal fields are
355 characteristically ^{13}C -enriched relative to the atmosphere and thus *not* the cause of the observed
356 isotopic shifts. However, some Southern Hemisphere coalfield emissions from open cast
357 bituminous mines may have contributed to the observed isotopic shift.

358
359 *Ascension – the remote marine tropics*

360 Ascension lies in the heart of the southern tropics, remote from any landmass, and thus
361 interpretation of its methane record must take note of events in the remote source regions of
362 winds reaching the island, especially in South America (see Fig. SI 2). The Ascension $\delta^{13}\text{C}_{\text{CH}_4}$
363 record shows a marked change beginning in late 2010, when strong growth was accompanied by
364 a sharp isotopic shift to more depleted $\delta^{13}\text{C}_{\text{CH}_4}$, in parallel with a comparatively subdued CO
365 cycle, albeit with excursions. The Cape Point and South Pole records are similar to the
366 Ascension pattern (Fig. 3 and Figs. SI 5 and SI 6). A distant source of air reaching Ascension is
367 Amazonia south of the ITCZ. In 2010, Amazonia experienced a major drought and biomass
368 burning. It is possible the early 2010 rise in methane at Ascension (Fig. 3) may have been driven
369 by biomass burning (Crevoisier et al., 2013), consistent with the observed enrichment of $\delta^{13}\text{C}_{\text{CH}_4}$
370 in early to mid-2010, both typical results of C4 savanna grassland fires. However, the seasonal
371 timing is perplexingly early in the southern winter. Trajectory studies suggest such emissions
372 would take some time to mix to Ascension, south of the ITCZ.

373
374 The Ascension observational record during this southern summer of 2010-11 is most simply
375 interpreted as the result of the very strong regional Southern Hemisphere wet season in Nov.
376 2010-March 2011, with subsequent very high Amazon flood levels in the first half of 2011 (Fig.
377 SI 12). Precipitation and perhaps also warmth in the wetlands may have driven a major emission
378 pulse of isotopically strongly depleted methane during the later (wetland-filling) part of the
379 Southern Hemisphere wet season, in March-June. This was a period so wet across the equatorial
380 and southern tropics that ocean levels dropped (Boening et al., 2012). Subsequent years were
381 also wetter than average: record Amazon flood levels were repeatedly observed in 2012, 2013,
382 and again in 2014, when there was heavy precipitation in the eastern flanks of the Andes in
383 Bolivia and Peru, with exceptional flood levels in the Amazon wetlands of Bolivia in 2007,
384 2008, and 2014 (Ovando et al., 2015) (see also SI section 12 and Fig. SI12). The South American
385 tropics have experienced rising temperatures and increased wet-season precipitation post-2000
386 (Gloor et al., 2013, 2015), which would further drive increasing emissions of methane,
387 particularly in the very hot year of 2014 (Gedney et al., 2004). Wetlands in Angola, Zambia and
388 Botswana likely experienced also high precipitation, as evidenced by flood levels in Lake Kariba
389 and the Okavango River in Botswana (Supp Info. Section 15).

390
391 *Wetlands and Agriculture*

392 Dlugokencky et al. (2009) found that the most likely drivers of methane growth in 2007-8 were
393 high temperatures in the Arctic and high precipitation in the tropics. In the years since then,
394 much of the growth has a tropical geographic locus, while the isotopic evidence implies fossil
395 fuel emissions were not the dominant driver. This suggests that tropical wetland or agricultural
396 emissions or a combination of both are the likely dominant causes of the global methane rise

397 from 2008-2014. There is much evidence that the variations in the global methane budget are
398 strongly dependent on tropical wetland extents and temperatures (Bousquet et al., 2006).

399
400 Tropical wetlands produce around 20-25% of global methane emissions: taking the mean of
401 many models of emissions in 1993-2004 Melton et al. (2013) found wetlands in the 30°N-30°S
402 latitude belt produced 126 ± 31 Tg CH_4 yr^{-1} . Wetland methane emissions respond quickly to
403 meteorological changes in temperature as emission has an exponential dependence on
404 temperature (Gedney et al., 2004; Westerman and Ahring, 1987) and precipitation (expanding
405 wetland area at the end of the rainy season). Methane emission responds rapidly to flooding and
406 warmth (Bridgham et al., 2013), with lags of a few days between flooding and emission
407 (Chamberlain et al., 2016), and methanogenic consortia have high resilience to drought periods.
408 Bousquet et al. (2016) found that variation in wetland extent could contribute 30-40% of the
409 range of wetland emissions. Emissions show strong seasonality, following the passage of the
410 ITCZ. Savanna wetlands fill in the late rainy seasons, after groundwater has been replenished,
411 typically in February to April in the Southern tropics and August to October in the Northern
412 Hemisphere tropics.

413
414 Hodson et al. (2011) showed that a large fraction of global variability in wetland emissions can
415 be correlated with the El Niño-Southern Oscillation (ENSO) index. For example, in the La Niña
416 years of 2007 and 2008, there is evidence that methane emissions from some Amazonian
417 wetland regions may have increased by as much as 50% (Dlugokencky et al., 2009) compared to
418 2000-2006. Amazon flood levels (see Fig. SI 12) were very high in 2009. In the La Niña of early
419 2011 (Boening et al., 2012), many southern tropical regions were unusually wet and equatorial
420 Amazon flood levels were again high. Amazon flooding also took place in 2012, 2013 and 2014.
421 In early 2014 (before the onset of the 2014 El Niño), extreme flood events occurred in the
422 Amazon wetlands of Bolivia (Ovando et al., 2015). Thus, summarizing, southern summer
423 wetland (Feb-April) or ruminant (Nov-April) emissions can lead to isotopically depleted
424 excursions, while winter (NH Dec-Mar; SH June-Sept) biomass burning of C4 grasslands
425 produces CO-rich air masses with isotopically enriched methane (Dlugokencky et al., 2011). The
426 response of emissions to temperature and the lag in wetland drying may in part account for
427 methane growth in some El Niño events (e.g. 1997), but this remains unexplained. In the
428 moderate *El Niño* event of 2006, Worden et al. (2011) showed that methane from Indonesian
429 fires could have compensated for an expected decrease in tropical wetland methane emissions
430 from reduced rainfall.

431
432 Agricultural emissions also respond to high rainfall, which supports rice agriculture and fodder
433 growth for ruminants, though widespread water storage and irrigation in the seasonal tropics is
434 now smoothing out the impact of year-to-year fluctuations. There is no evidence for a sudden
435 sharp increase in rice fields in 2007. Rice harvested area in Asia is increasing but fluctuates: in
436 1999 (an above-trend year) the area was 140.4 million ha, and 141.0 M ha in 2009 (a below-
437 trend year). By 2013 Asian rice field area harvested had risen to 146.9 M ha
438 (<http://ricestat.irri.org:8080/wrs2/entrypoint.htm>). In China, as an example, it is possible that rice
439 agriculture may have contributed to increased emissions, but there is no evidence for a step-
440 change in rice fields under cultivation: indeed, paddy field area harvested is relatively stable and
441 declined from 2006 to 2007 (<http://faostat.fao.org>). Tropical agricultural emissions from
442 ruminants are indeed likely to have increased in high rainy seasons, but if so, these increases

443 were probably mainly in South America and Africa. This is because in India, the nation with the
444 world's largest ruminant population, recent monsoons have mostly been average to poor, and
445 cattle populations have declined (see SI section 11).

446

447 **4.2 Methane sink variation?**

448 A possible explanation for global methane growth is that destruction rates reduced over this time
449 period. The global atmospheric burden of methane corresponding to 1 ppb is about 2.77 Tg of
450 methane. Reaction with tropospheric OH is the main methane sink: for example, a 1% change in
451 OH abundance, equivalent to a ~ 5 Tg $\text{CH}_4 \text{ yr}^{-1}$ change in methane emissions, or roughly 2 ppb
452 globally, could contribute significantly to an apparent 'source shift' over several years. OH
453 abundance is greatest in the bright sunlight of the moist tropical troposphere, and thus can vary
454 significantly with short-term changes in tropical meteorology and pollution. El Niño For
455 example, the major global wildfires during the intense El Niño event of 1997–1999 coincided
456 with, and likely caused, an OH minimum (Prinn et al., 2005; see also Duncan et al. 2003).

457

458 The long-term trend, if any, in OH abundances is not well understood (Prinn et al., 2005, Patra et
459 al., 2014), but there is evidence for OH having small interannual variations (Montzka et al.,
460 2011). OH is well buffered in the tropical upper troposphere (Gao et al., 2014), and globally OH
461 appears to have been stable within $\pm 3\%$ over 1985 – 2008: this result is more reliable from 1997
462 onward (Rigby et al., 2008). Rigby et al. (2008) inferred a large, but uncertain, decrease in OH in
463 2007 ($-4 \pm 14\%$), implying that part of the growth in methane mole fraction in 2007 may have
464 been driven by a smaller sink, however, that work had not considered the isotopic CH_4 data.
465 During 2006–8, OH may have only varied by less than 1% globally, although larger regional
466 changes may have occurred, with some evidence for low OH over the western Pacific warm pool
467 (Rex et al., 2013). Thus there is little *prima facie* evidence that a major change in OH has driven
468 methane's rise and isotopic shift. Methane removal by the atomic Cl sink, discussed in SI
469 Section 16, is also unlikely to explain the observed changes.

470

471 **5. Running budget analysis and interpretation of shifts in the $\delta^{13}\text{C}_{\text{CH}_4}$ record**

472 An objective analysis of the cause for the recent rise in methane requires a balanced
473 consideration of changes in sources or removal rates. Fig. 4 summarises the changes with time of
474 mole fraction and $\delta^{13}\text{C}_{\text{CH}_4}$ over the period since 1998. The importance of $\delta^{13}\text{C}_{\text{CH}_4}$ data for
475 identifying such changes in CH_4 sources or removal rates is becoming increasingly clear
476 (Monteil et al., 2011; Ghosh et al., 2015).

477

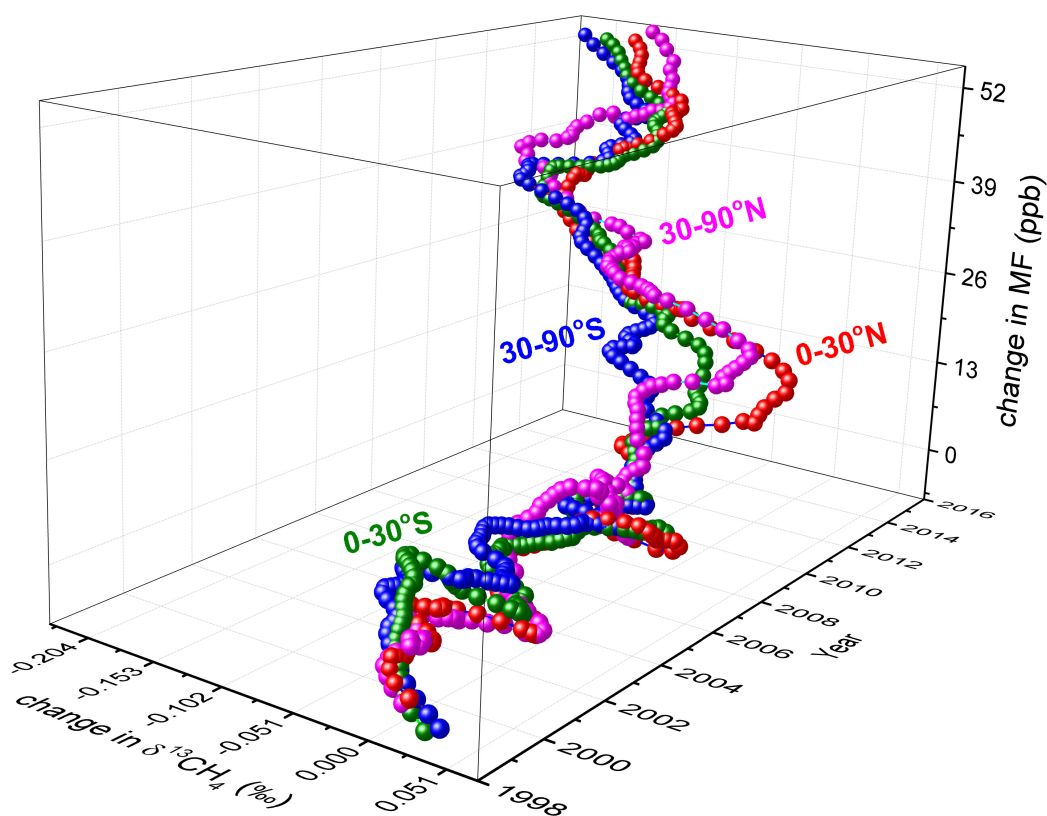
478 To consider how the most recent data can clarify explanations for the increase in mole fraction
479 together with the striking concurrent reversal of the long term trend for increasing $\delta^{13}\text{C}_{\text{CH}_4}$ over
480 the last hundred years, a latitudinally-zoned monthly budget analysis is carried out here. Two
481 hypotheses to explain the recent changes in the methane mole fraction and isotopic records are
482 considered: a) "changes in emissions" or b) "changes in removal rates". The second option also
483 considers whether a spatial redistribution of removal rates can explain the recent changes in
484 atmospheric CH_4 .

485

486 There are still significant uncertainties in the CH_4 budget, as shown by the bottom up estimates
487 for emissions from natural sources over 2000 – 2009 being 50% larger than their top down
488 estimates and the range of estimates for anthropogenic emissions being 100% larger for top

489 down estimates than for bottom up estimates (Ciais et al., 2013). However, the focus here is to
 490 consider how recent changes in the budget can cause a transition from the relatively stable period
 491 over 1999 – 2006 to significant increases in mole fraction together with decreases in $\delta^{13}\text{C}_{\text{CH}_4}$
 492 over 2007 – 2014. This is done by considering the magnitudes and timings of changes to a
 493 central estimate for the top down budget (Kirschke et al. 2013; Ciais et al. 2013) which can
 494 explain the observations. This is not designed to improve our understanding of the total budget
 495 but rather to assess how much it has to change to explain recent data.

496
 497 A simple running budget analysis is used here to compare how variations in CH_4 emissions or in
 498 its removal rate can explain the observed changes in mole fraction and $\delta^{13}\text{C}_{\text{CH}_4}$ data. The focus is
 499 on 1998 – 2014. However, NOAA mole fraction data from 1983, together with ice core and firn
 500 air data (Ferretti et al., 2005), and earlier NIWA $\delta^{13}\text{C}_{\text{CH}_4}$ data over 1992 – 1997 (Lassey et al.,
 501 2000) have also been used to carry out a spin-up phase for this analysis.



502
 503
 504 Figure 4. 3-D graphic for changes in $\delta^{13}\text{C}_{\text{CH}_4}$ and mole fraction with time, showing mid points
 505 for the years marked. MF – mole fraction. Colour code: Blue = 30-90°S, Green = 0-30°S, Red =
 506 0-30°N, Mauve = 30-90°N.

507
 508 Monthly average mole fraction and $\delta^{13}\text{C}_{\text{CH}_4}$ data are used to determine the total emissions and
 509 their $\delta^{13}\text{C}$ values for four semi-hemisphere regions (30-90°S, 0-30°S, 0-30°N, 30-90°N) but
 510 with the focus being on long term trends and major year-to-year variations around these, rather
 511 than specific regional effects. CH_4 mixes within each hemisphere over periods of a few months
 512 and between hemispheres over about one year. As shown in Figures SI.3 and SI.14, this leads to

513 a fairly stable spatial distribution modulated by seasonal cycles that depend on location but have
 514 relatively small interannual variations (Dlugokencky et al., 1994). Cubic spline fits to the CH₄
 515 data for the four regions are then used to compare how monthly variations in emissions or in
 516 removal rates can reproduce the data over 1998 - 2014.

517
 518 Interannual variations are shown by using running 12-month means to remove the seasonal cycle
 519 for the observed mole fraction data in Fig 5 and for $\delta^{13}\text{C}_{\text{CH}_4}$ in Fig 6. However, the budget
 520 analysis is fitted to monthly data, as shown in SI section 16, in order to cover seasonal cycles in
 521 emissions and removal rates that have non-linear effects on isotope ratios.

522
 523 The differential equations used here to relate mole fractions to emissions and removal rates are:

$$524 \quad \frac{d}{dt} C_i = S_i - K_i C_i - \sum_j X_{ij} (C_i - C_j) \quad [1]$$

525 Where i denotes a region, C_i are mole fractions in units of ppb, S_i are emission rates in units of
 526 ppb/yr, K_i are removal rates (1/yr), and X_{ij} are exchange rates between the one or two adjacent
 527 regions. The differential equations used for $\delta^{13}\text{C}_{\text{CH}_4}$ are similar to Lassey *et al.* (2000) where
 528 simpler differential equations for $^{13}\text{C}/\text{C}$, are treated by using systematic differences between
 529 $^{13}\text{C}/^{12}\text{C}$ and $^{13}\text{C}/\text{C}$ ratios as:

$$530 \quad [^{13}\text{CH}_4] = (1 + \delta) R_{\text{PDB}} [^{12}\text{CH}_4] = \frac{(1 + \delta) R_{\text{PDB}}}{[1 + (1 + \delta) R_{\text{PDR}}]} C_i = (1 + \delta') R_{\text{PDB}} C_i \quad [2]$$

531 where $R_{\text{PDB}} = 0.0112372$ for the VPDB standard, and δ' applies to the $^{13}\text{C}/\text{C}$ ratios. The
 532 differential equations for $^{13}\text{CH}_4$ mole fractions, now written as F_i , are then:

$$533 \quad \frac{d}{dt} F_i = (1 + \delta'_{S_i}) R_{\text{PDB}} S_i - (1 + \varepsilon) K_i (1 + \delta'_i) R_{\text{PDB}} C_i - \sum_j X_{ij} (F_i - F_j) \quad [3]$$

535 where δ'_{S_i} are for the source $^{13}\text{C}/\text{C}$ ratios, and ε is the KIE for the removal rate. This can then be
 536 simplified to:

$$537 \quad \frac{d}{dt} \delta'_i = (\delta'_{S_i} - \delta'_i) (S_i / C_i) - \varepsilon K_i - \sum_j X_{ij} (\delta'_i - \delta'_j) (C_j / C_i) \quad [4]$$

538 While equation [1], and its equivalent for $[^{13}\text{CH}_4]$ used in some analyses (Schaefer *et al.* 2016)
 539 are linear equations, [4] makes it clear that the δ' have non-linear relationships with the S_i and C_i .

540
 541 Mole fraction data from 51 NOAA sites together with $\delta^{13}\text{C}_{\text{CH}_4}$ data from 20 NOAA sites and 2
 542 RHUL sites are used but because of limited spatial coverage for $\delta^{13}\text{C}_{\text{CH}_4}$ data, monthly averages
 543 over four semi-hemispheres, covering 0-30° and 30-90° zonal regions, are used to determine
 544 corresponding emissions, removal and transport. The CH₄ emissions and their $\delta^{13}\text{C}$ values are
 545 fitted to the observed mole fraction and $\delta^{13}\text{C}_{\text{CH}_4}$ data using a range of estimates for removal rates
 546 consistent with the last IPCC assessment report (Ciais et al., 2013), but covering options for
 547 spatial and seasonal distributions of the removal by soils, tropospheric Cl and cross tropopause
 548 transport which are less well defined than they are for removal by OH. Interannual variations in
 549 exchange rates between the regions are also considered as another option. Then for comparison
 550 an alternative set of model runs allows interannual variations in the removal rate over 1998 –
 551 2014, while keeping the emissions fixed after 1999. In both cases this is a simple form of inverse

552 modelling that avoids prior estimates of the source budget and treats interannual variations in
 553 either source emissions or in removal rates equally. More details of the data averaging and
 554 running budget analysis are provided in Table 1 and in SI section 16.

555

556

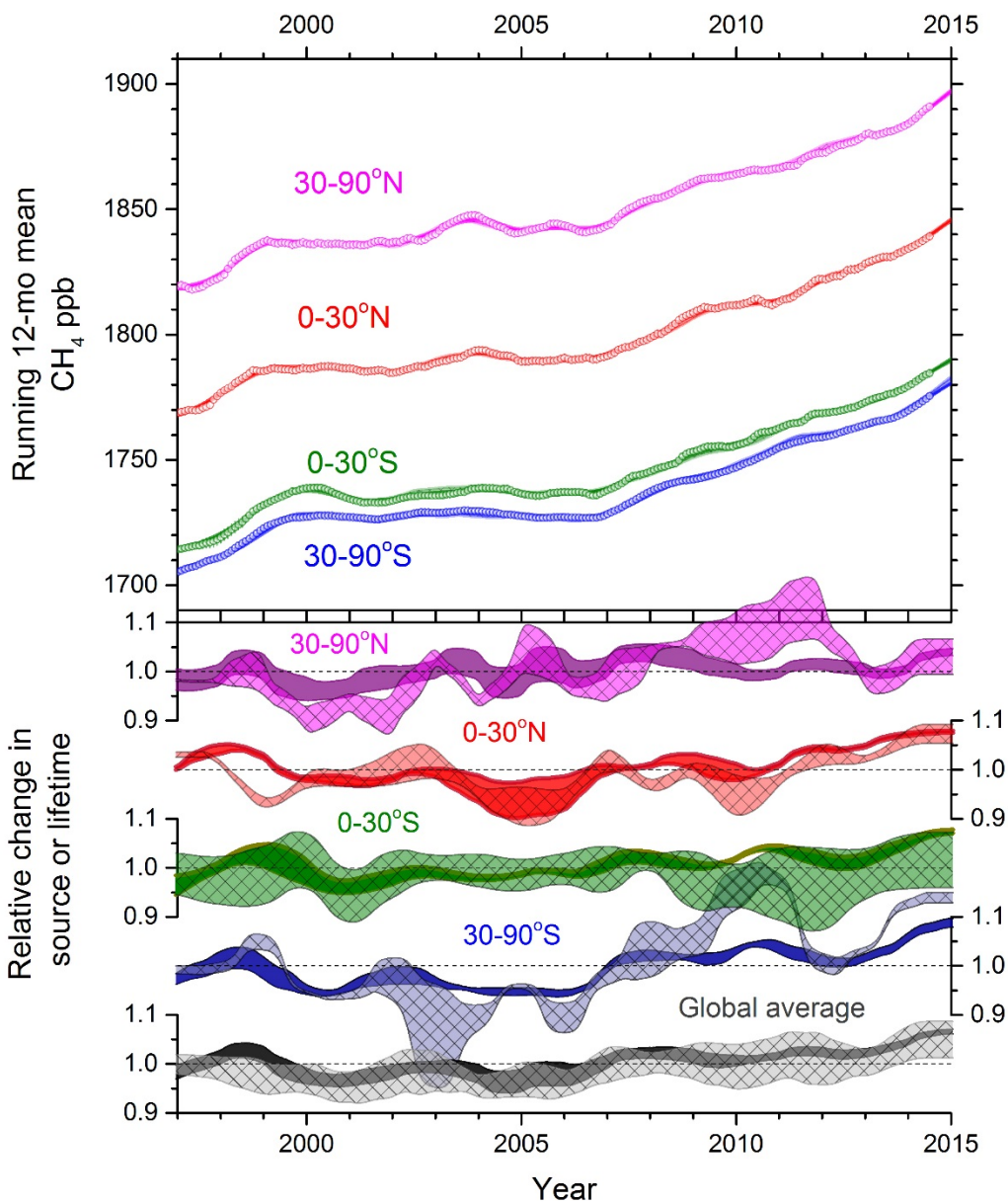
557

558

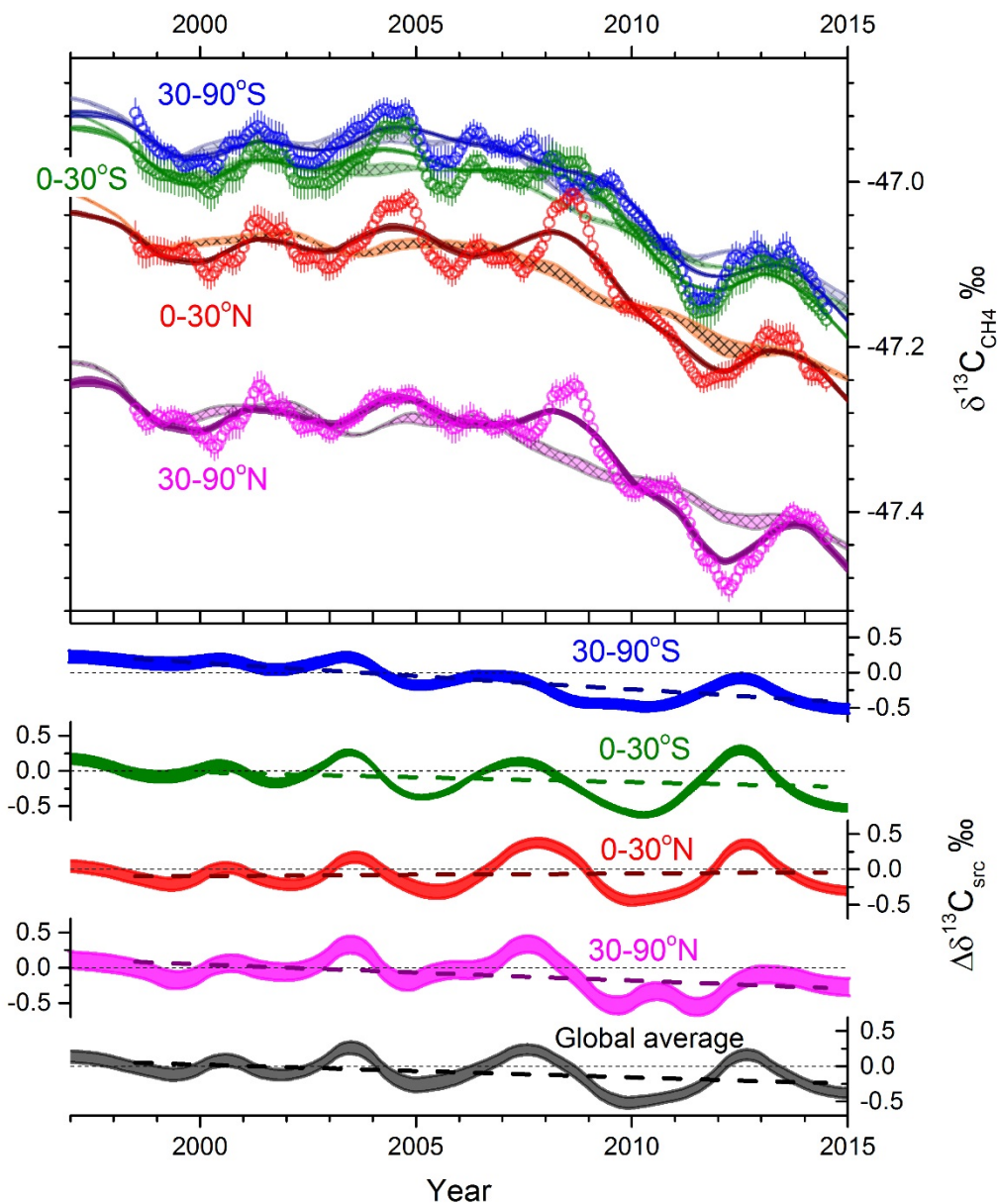
Table 1. The range of options considered in determining fits of source emissions or of removal rates to the regional mole fraction and $\delta^{13}\text{C}_{\text{CH}_4}$ data.

Seasonal cycles				
OH removal	Spivakovsky et al., 2000			
Cl removal	Constant	Same as OH		
Soil removal	Constant	Same as OH		
Cross tropopause transport	Constant			
Source emissions	Fitted to data for each region, no interannual variability			
Source $\delta^{13}\text{C}$	Fitted to data for each region, no interannual variability			
Spatial distributions				
OH removal	Spivakovsky et al., 2000			
Cl removal	Uniform	SH only		
Soil removal	proportional to land area			
Cross tropopause transport	Uniform	Low latitudes only		
Interannual variations				
	<i>1. Source fits</i>		<i>2. Removal rate fits</i>	
Removal rates	No change		Vary over 1992 – 2014	
Source emissions	Vary over 1990 – 2014		Vary over 1990- 1998	
Source $\delta^{13}\text{C}_s$	Vary over 1998 – 2014		Vary over 1990- 1998	
Exchange rates 1990 - 2014	Fixed	Varying	Fixed	Varying

559



560
 561 Fig 5. The upper panel shows running 12-month means of methane mole fractions from the
 562 NOAA Cooperative Global Air Sampling Network averaged over 0-30° and 30-90° latitude
 563 regions in each hemisphere (see SI section 16). Uncertainty bands around these running means
 564 show the range of mole fraction values that remain after correcting for average site differences.
 565 Ranges for fits to the data are shown using changes in either CH₄ source emissions (darker) or in
 566 removal rates (lighter), however, as each give good fits to the mole fractions these are hard to
 567 distinguish. The lower panels show the corresponding ranges for relative changes in zonal CH₄
 568 source emissions (darker) or lifetimes, i.e. the inverse of removal rates, (lighter and
 569 crosshatched) for each region and for the global average. See text for source emission and
 570 removal rate ranges.
 571



572 Fig 6. The upper panel shows running 12-month means for $\delta^{13}\text{C}_{\text{CH}_4}$ from the NOAA and RHUL
 573 sites that have also been combined to represent averages over the four regions. Results from the
 574 budget analysis are shown for changes in source emissions (darker) or removal rates (lighter and
 575 cross-hatched) as in Fig 5. The lower panels show the corresponding variations in source $\delta^{13}\text{C}$
 576 (‰) for the four regions and for the global average source $\delta^{13}\text{C}$.
 577

578 *Mole Fraction Constraints.* Most of the variation in mole fraction data can be explained by either
 579 of the two hypotheses: "changes in source emissions" or "changes in removal rates", or a
 580 combination of both. Models assuming 'changes in emissions' only, and 'changes in removals'
 581 only are shown in Fig. 5. While there are some systematic differences between data and fits, the
 582 residuals are only slightly larger for the "changes in removal" option.

583 The “changes in source emissions” model shown in Fig 5 has emissions in the range 560 - 580
584 Tg CH₄ yr⁻¹ when averaged over 1998 - 2014, similar to values of Kirschke et al. (2013), with
585 11% in the 30–90°S region, 27% in 0–30°S, 32% in 0–30°N and 30% in 30–90°N. There is a
586 source trend of 0.8 to 1.5% yr⁻¹ in the 0–30°N region over 2005 to 2014 in contrast to the 30–
587 90°N that has a trend of -0.5 to +0.1% yr⁻¹ over this period. In the 0–30°S region this trend is 0.4
588 to 0.5% yr⁻¹ and in the 30–90°S region it is 0.8 to 0.9 % yr⁻¹. The larger relative variations for
589 30-90°S may reflect this zone's emissions being small relative to the global total making it more
590 sensitive to variations in transport such as an increasing extent of Hadley circulation (Tselioudis
591 et al., 2016). Total source increases over this period are in the range of 3 to 6% and
592 predominantly in the 0–30°S and 0–30°N regions. These source changes are described in more
593 detail in SI Section 16 and are consistent with other estimates (Dlugokencky et al., 2009;
594 Bousquet et al., 2011) but have now been continuing for nine years.

595 If, alternatively, "changes in removal rates" (or lifetimes) are used to explain the CH₄ mole
596 fraction data, then significantly larger relative variations are needed than for source variations,
597 however, this is partly due to the constraints also being imposed by the δ¹³C_{CH4} data as shown
598 below. Over 1998 – 2014, variations of 7% – 10% are used in the low latitudes and 15% – 25%
599 in the high latitudes. In particular, the slowdown in CH₄ growth rate over 2009 – 2011 requires
600 very large increases in the lifetimes in high latitudes and some compensating reduction in
601 lifetimes in the low latitudes. Relative changes in the global mean lifetime are smaller because of
602 these compensating effects, but it still requires an increase of ~10% over 2000 – 2014. This is
603 much larger than expected fluctuations of OH radicals (Montzka et al. 2011). Furthermore,
604 because cross tropopause transport is expected to remove ~8% of CH₄ while reaction with Cl and
605 the soil sink each account for 4 – 5% (Ciais et al. 2013), variations in removal rate that are
606 required to explain the observed mole fraction data cannot be explained without some significant
607 changes in OH.

608
609 *Isotopic Constraints.* An even clearer distinction between the two modelled hypotheses is shown
610 when isotopes are considered (Fig 6). The shift in the bulk δ¹³C_{CH4} value of the global source is
611 about -0.17‰. The "changes in source emissions" option follows the interannual variations in
612 δ¹³C_{CH4} much better than the "changes in removal rates" option and this is more obvious in the
613 northern hemisphere where these variations are large. Furthermore, variations in removal rates
614 cannot explain the large positive anomalies in 2004 and 2008 or the large negative anomaly over
615 2011 – 2012.

616
617 Source δ¹³C values averaged over 1998 – 2014 for the regions are in the ranges: -57.8 ± 0.05‰
618 for 30-90°S; -53.9 ± 0.04‰ for 0-30°S; -51.9 ± 0.07‰ for 0-30°N; and -53.4 ± 0.13‰ for 30-
619 90°N. In addition to significant interannual variations mentioned above there is also clearly a
620 longer term trend of decreasing δ¹³C_{CH4} values. Fig 6 shows that this corresponds to a decrease
621 in source δ¹³C values that started five to ten years earlier as would be expected because of the
622 significant lag in the δ¹³C_{CH4} response to change (Tans, 1997). The most obvious trends in source
623 δ¹³C are in the 30-90°S and 30-90°N regions but there is also a negative trend in the 0–30°S
624 region (see also Fig, SI 4). This spatial pattern for trends in source isotopic signatures may relate
625 to the long term decrease in biomass burning over this period (Le Quéré et al., 2014) at the same
626 time as an increase in wetland emissions (Bousquet et al., 2011). Also the timing for this change
627 in source δ¹³C values is consistent with satellite data showing trends in land surface open water

628 areas that decreased from 1993 to 2002 but then started to increase (Prigent et al., 2012).

629
630 While an increase in lifetimes, i.e. decrease in removal rates by OH and other sinks, could
631 reproduce the long term decrease in $\delta^{13}\text{C}_{\text{CH}_4}$, this analysis shows that it requires major changes in
632 the global average removal rate as well as large fluctuations in the four semi-hemispheres, while
633 still not accounting for much of the year-to-year interannual variations. The extent to which
634 reversal of the long term trend in $\delta^{13}\text{C}_{\text{CH}_4}$ could be caused by a decrease in OH is heavily
635 constrained by the more direct tracers of OH which suggest that it has no long term trend
636 (Montzka et al., 2011). However, a much larger fractionation occurs in removal by soil
637 methanotrophy and this can be anticorrelated with methanogenesis (Bridgham et al., 2013) so
638 that changes in wetlands could be having a larger relative effect on the seasonal cycle for $\delta^{13}\text{C}_{\text{CH}_4}$
639 than for the mole fraction. Furthermore, the large isotopic fractionation due to reaction with Cl in
640 the marine boundary layer is sensitive to temperature and this may lead to interannual variability
641 that may have been recognised in some data not included here (Allan et al., 2005).

642 **6 Conclusions**

643 The $\delta^{13}\text{C}_{\text{CH}_4}$ isotopic shifts reported here and the likelihood that changes in the OH methane sink
644 are not consistent with the observed trends, suggest that from 2007 growth in atmospheric
645 methane has been largely driven by increased biogenic emissions of methane, which is depleted
646 in ^{13}C . Both the majority of this methane increase and the isotopic shift are biogenic. This growth
647 has been global but, apart from 2007, has been led from emissions in the Tropics and Southern
648 Hemisphere, where the isotopically depleted biogenic sources are primarily microbial emissions
649 from wetlands and ruminants, with the trend in source $\delta^{13}\text{C}_{\text{CH}_4}$ in the 0–30°S zone being
650 particularly significant.

651
652 While significant uncertainties in the global methane budget still remain, our top down analysis
653 has shown that relative increases in the global average emissions of 3 – 6% together with a shift
654 of about -0.17‰ in the bulk $\delta^{13}\text{C}_{\text{CH}_4}$ value of the global source over the last twelve years can
655 explain much of the observed trends in methane's mole fraction and $\delta^{13}\text{C}_{\text{CH}_4}$ values. Alternative
656 explanations, such as increases in the global average atmospheric lifetime of methane would
657 have to have been an unrealistic 5 – 8% over this period and cannot explain the interannual
658 variations observed in $\delta^{13}\text{C}_{\text{CH}_4}$.

659
660 Although fossil fuel emissions have declined as a proportion of the total methane budget, our
661 data and results cannot rule out an increase in absolute terms, especially if the source gas were
662 isotopically strongly depleted in ^{13}C : however, both the latitudinal analysis and isotopic
663 constraints rule out Siberian gas, which is around -50‰ (Dlugokencky et al. 2011), as a cause of
664 the methane rise, and emissions from other fossil fuel sources such as Chinese coal, US fracking
665 or most liquefied natural gas are more enriched in ^{13}C and thus also do not fit the isotopic
666 constraints.

667
668 The evidence presented here, and in the Supplementary Information, is that the growth, isotopic
669 shift, and geographic location coincide with the unusual meteorological conditions of the past 9
670 years, especially in the tropics. These events included the extremely warm summer and autumn
671 in 2007 in the Arctic, the intense wet seasons in the Southern Hemisphere tropics under the ITCZ
672 in late 2010-11 and subsequent years, and also the very warm year of 2014. The monsoonal 0°-

673 30°N Northern Hemisphere, probably especially in South and East Asia (Nisbet et al., 2014,
674 Patra et al., 2015), also contributed to post-2011 growth.

675
676 Schaefer et al. (2016), using a one-box model, considered but rejected the hypothesis that
677 wetland emissions have been the primary cause of methane growth. This was on the basis of
678 remote sensing data that suggested growth was led from the northern hemisphere and also
679 isotopic arguments, as they assumed tropical ruminants were C3-fed. They preferred the
680 hypothesis that growth has been driven by agricultural emissions, but commented that the
681 evidence was ‘not strong’. The evidence presented here for the latitudinal distribution of growth
682 suggests that southern hemisphere wetland emissions may have been more important than
683 thought by Schaefer et al. (2016).

684
685 Our study concurs with Schaefer et al. (2016) that the methane rise is a result of increased
686 emissions from biogenic sources. The location and strong interannual variability of the methane
687 growth suggest that a fluctuating natural source is predominant rather than an anthropogenic one.
688 Rice field and ruminant emissions have likely contributed significantly to the rise in tropical
689 methane emissions, but rice-harvested areas and animal populations change slowly and there is
690 little evidence for a step-change in 2007 that is capable of explaining the trend-change in the
691 methane record. Consequently while agricultural emissions are likely to be increasing, as
692 postulated by Schaefer et al. (2016), and probably have been an important component in the
693 recent increase, we find that tropical wetlands are likely the dominant contributor to recent
694 growth.

695
696 Schaefer et al. (2016) raised the troubling concern that the need to control methane emissions
697 may conflict with food production. They warned that, “if so, mitigating CH₄ emissions must be
698 balanced with the need for food production”. This is a valid concern, but we believe that changes
699 in tropical precipitation and temperature may be the major factors now driving methane growth,
700 both in natural wetlands and in agriculture.

701
702 Renewed growth in atmospheric methane has now persisted for 9 years. The methane record
703 from 1983-2006 (Fig. 1) shows a clear trend to steady state (Dlugokencky et al. 2009,
704 Dlugokencky et al. 2011), apart from ‘one-off’ events, such as the impact of the Pinatubo
705 eruption in 1991-1992, and the intense El Niño of 1997-1998. But the current growth is different,
706 and has been sustained since 2007, although the modelling work presented above suggests that
707 the present trend to more isotopically depleted values may have started in the last years of the
708 previous century. The abrupt timing of the change in growth trend in 2007 is consistent with a
709 hypothesis that the growth change was primarily in response to meteorological driving factors.
710 Changes in emissions from anthropogenic sources, such as fossil fuels, agricultural ruminant
711 populations and area of rice fields under cultivation, would be more gradual. The strong isotopic
712 shifts measured in late 2010-2011 are consistent with a response to the intense La Niña. The
713 exceptional global methane increase in 2014 (Fig. 1) was accompanied by a continuation of the
714 recent isotopic pattern (Figs. 2, 3 and SI 10).

715
716 The scale and pace of the present methane rise (roughly 60 ppb in 9 years since the start of
717 2007), and the concurrent isotopic shift showing that the increase is dominantly from biogenic
718 sources, imply methane emission (both from natural wetlands and agriculture) is responding to a

719 sustained changes in precipitation and temperature in the tropics. If so, is this merely a decadal-
720 length weather oscillation, or is it a troubling harbinger of more severe climatic change? Is the
721 current sustained event in the normal range of meteorological fluctuation? Or is a shift occurring
722 that is becoming comparable in scale to events recorded in ice cores (Wolff and Spahni, 2007;
723 Möller et al., 2013, Sperlich et al., 2015). In the past millennium between 1000-1700 C.E,
724 methane mole fraction varied by no more than about 55 ppb (Ferretti et al., 2013). Methane in
725 past global climate events has been both a 'first indicator' and a 'first responder' to climatic
726 change (Severinghaus and Brook, 1999; Möller et al., 2013; Etheridge et al., 1998). Comparison
727 with these historic events suggests that if methane growth continues, and is indeed driven by
728 biogenic emissions, the present increase is already becoming exceptional, beyond the largest
729 events in the last millennium.

730 **Acknowledgments and Data**

731 We thank the UK Meteorological Office for flask collection and hosting the continuous
732 measurement at Ascension, the Ascension Island Government for essential support, and
733 Thumeka Mkololo for flask collection in Cape Town.

734

735 **Data sources and archiving are listed in the Supporting Information section 2.**

736 **References**

- 737 Berchet, A., et al. (2015) Atmospheric constraints on the methane emissions from the East
738 Siberian Shelf *Atmos. Chem. Phys. Discuss.*, 15, 25477-25501.
- 739 Bergamaschi, P. et al. (2013) Atmospheric CH₄ in the first decade of the 21st century: inverse
740 modeling analysis using SCIAMCHY satellite retrievals and NOAA surface measurements. *J.*
741 *Geophys. Res.* 118, 7350-7369.

- 742 Boening, C. et al. (2012) The 2011 La Niña: so strong the oceans fell. *Geophys. Res. Lett.* 39,
743 L19602
- 744 Bousquet, P. et al. (2006) Contribution of anthropogenic and natural sources to atmospheric
745 methane variability. *Nature*, 443, 439-443.
- 746 Bousquet, P. et al. (2011) Source attribution of the changes in atmospheric methane for 2006-
747 2008. *Atmos. Chem. Phys.* 11, 3689-3700.
- 748 Bousquet, P. et al. (under open review 2016) The Global methane budget, 2000-2012. *Earth*
749 *System Science Data Disc.* doi:10.5194/essd-2016-25, 2016.
- 750 Bridgham, S. D., Cadillo-Quiroz, H., Keller, J.K and Zhuang, Q.. (2013) Methane emissions
751 from wetlands: biogeochemical, microbial, and modeling perspectives from local to global
752 scales. *Glob. Change Biol.* 19, 1325-1346
- 753 Bruhwiler, L/M. et al. (2014) CarbonTracker-CH₄: an assimilation system for estimating
754 emissions of atmospheric methane. *Atmos. Chem. Phys.*, 14, 8269-8293.
- 755 Chamberlain, S.D. et al. (2016) Influence of transient flooding on methane fluxes from sub-
756 tropical pastures. *J. Geophys. Res, Biogeosciences.* 121, 965-977.
- 757 Ciais, P., et al., (2013) Chapter 6: Carbon and Other Biogeochemical Cycles. In: *Working Group*
758 *I Contribution to the IPCC Fifth Assessment Report (AR5), Climate Change 2013: The*
759 *Physical Science Basis* [T. Stocker, D. Qin, G.-K. Plattner, et al. (eds.)]. Cambridge University
760 Press.
- 761 Comiso, J.C. and Nishio, F. (2008) Trends in the sea-ice cover using enhanced and compatible
762 AMSR-E, SSM/I, and SMMR data. *Geophys. Res. Lett.* 35, L031972
- 763 Crevoisier, C. et al. (2013) The 2007-2011 evolution of tropical methane in the mid-troposphere
764 as seen from space by MetOp-A/IASI. *Atmos. Chem. Phys.*, 13, 4279–4289.
- 765 Dlugokencky E.J., Masarie, K.A., Lang, P.M. and Tans, P.P. (1998) Continuing decline in the
766 growth rate of atmospheric methane. *Nature* 393, 447-450
- 767 Dlugokencky, E. J., Myers, R. C., Lang, P. M., Masarie, K. A., Crotwell, A. M., Thoning, K. W.,
768 Hall, B. D., Elkins, J. W., and Steele, L. P.(2005) Conversion of NOAA atmospheric dry air
769 CH₄ mole fractions to a gravimetrically prepared standard scale, *J. Geophys. Res.*, 110,
770 D18306.
- 771 Dlugokencky, E.J. et al. (2009) Observational constraints on recent increases in the atmospheric
772 CH₄ burden. *Geophys. Res. Lett.*, 36, L18803
- 773 Dlugokencky, E.J., Nisbet, E.G., Fisher, R.E. and Lowry, D. (2011) Global atmospheric
774 methane: budget, changes, and dangers. *Phil. Trans. R. Soc. A.* 369, 2058–2072
- 775 Duncan, B.N. et al. (2003) Interannual and seasonal variability of biomass burning emissions
776 constrained by satellite observations. *J. Geophys. Res.* 108, doi.10.1029/2002JD002378.
- 777 Etheridge, D.M., Steele, L.P., Francey, R.J. and Langenfelds, R.L. (1998) Atmospheric methane
778 between 1000 A.D. and present: Evidence of anthropogenic emissions and climatic variability.
779 *J. Geophys. Res.*, 103, 15979-15993
- 780 Ferretti, D.F. et al. (2005) Unexpected changes to the global methane budget over the past 2000
781 years. *Science*, 309, 1714
- 782 Fisher, R.E. et al. (2011) Arctic methane sources: isotopic evidence for atmospheric inputs
783 *Geophys. Res. Lett.* 38, L21803
- 784 Galimov, E.M. and Rabbani, A.R. (2001) Geochemical characteristics and origin of natural gas
785 in southern Iran. *Geochem. Int.*, 39, 780-792.

- 786 Gao, R.S. et al. (2014) OH in the tropical upper troposphere and its relationships to solar
787 radiation and reactive nitrogen. *J. Atmos. Chem.* 71, 55-64
- 788 Gedney, N. et al. (2004) Climate feedback from wetland methane emissions. *Geophys. Res. Lett.*
789 31, L20503.
- 790 Ghosh, A. et al. (2015) Variations in global methane sources and sinks during 1910-2010. *Atmos.*
791 *Chem. Phys.* 15, 2595-2612
- 792 Gloor, M. et al. (2013) Intensification of the Amazonian hydrological cycle over the last two
793 decades. *Geophys. Res. Lett.*, 40, 50377
- 794 Gloor, M. et al. Recent Amazon climate as background for possible ongoing and future changes
795 of Amazon humid forests (2015), *Global Biogeochemical Cycles*, doi: 10.1002/2014GB005080
- 796 Hamilton, S.K., et al. (2014) Stable isotopic and molecular composition of desorbed coal seam
797 gases from the Walloon Subgroup, eastern Surat Basin, Australia. *Int. J. Coal Geology*, 122, 21-
798 36.
- 799 Kay, J.E. et al. (2007) The contribution of cloud and radiation anomalies to the 2007 Arctic Sea
800 Ice minimum. *Geophys. Res. Lett.* 35, L08503.
- 801 Kirschke, S. et al. (2013) Three decades of global methane sources and sinks *Nature Geosci.* 6,
802 813-823.
- 803 Le Quéré, C. et al. (2014) Global carbon budget 2013. *Earth System Science Data* 6, 235-263
- 804 Melton, J.R. (2013) Present state of global wetland extent and wetland methane modeling:
805 conclusions from a model intercomparison project (WETCHIMP) *Biogeosciences*, 10, 753-
806 788.
- 807 Min, S.-K., and Son, S.-W. (2013) Multimodal attribution of the Southern Hemisphere Hadley
808 cell widening: major role of ozone depletion. *J. Geophys. Res.* 118, 3007-3015
- 809 Möller, L. et al. (2013) Independent variations of CH₄ emissions and isotopic composition over
810 the past 160,000 years. *Nature Geoscience*, 6, 885-890.
- 811 Monteil, G. et al. (2011) Interpreting methane variations in the past two decades using
812 measurements of CH₄ mixing ratio and isotopic composition. *Atmos. Chem. Phys.* 11, 9141-
813 9153
- 814 Montzka, S.A., (2011) Small interannual variability of global atmospheric hydroxyl. *Science*,
815 331, 67-69
- 816 Nisbet, E.G., Dlugokencky, E.J. and Bousquet, P. (2014) Methane on the rise – again. *Science*,
817 343, 493-5
- 818 Ovando, J. et al. (2015) Extreme flood events in the Bolivian Amazon wetlands. *J. Hydrology:*
819 *Regional Studies*, 5, 293-308.
- 820 Patra, P.K. et al. (2014) Observational evidence for inter-hemispheric hydroxyl-radical parity.
821 *Nature*, 513, 219-223
- 822 Patra, P.K. et al. (In Press) Regional methane emission estimation based on observed
823 atmospheric concentrations (2002-2012). *J. Met. Soc. Japan.* 94, 91-113.
- 824 Pickers, P.A. and Manning, A.C. (2015) Investigating bias in the application of curve fitting
825 programs to atmospheric time series. *Atmos. Meas. Tech.*, 8, 1469-1489.
- 826 Prigent, C. et al. (2012) Changes in land surface water dynamics since the 1990s and relation to
827 population pressure. *Geophys. Res. Letts*, 39, L08403.
- 828 Prinn, R.G. et al. (2005) Evidence for variability of atmospheric hydroxyl radicals over the past
829 quarter century. *Geophys. Res. Lett.*, 32, L022228.
- 830 Rex, M. et al. (2014) A tropical West Pacific OH minimum and implications for stratospheric
831 composition. *Atmospheric Chemistry and Physics*, 14, 4827-4841.

- 832 Rigby, M., et al. (2008) Renewed growth of atmospheric methane *Geophys. Res. Lett.*, 35,
 833 L22805.
- 834 Schaefer, H., et al., 2016: A 21st century shift from fossil-fuel to biogenic methane emissions
 835 indicated by $^{13}\text{CH}_4$. *Science*, 352, 80-84.
- 836 Severinghaus, J.P. and Brook, E.J. (1999) Abrupt Climate Change at the End of the Last Glacial
 837 Period Inferred from Trapped Air in Polar Ice. *Science*, 286, 930-934.
- 838 Sperlich, P. et al. (2015) Carbon isotope ratios suggest no additional methane from boreal
 839 wetlands during the rapid Greenland Interstadial 21.2. *Global. Biogeo. Cycles*
 840 10.1002/2014GB005007.
- 841 Spivakovsky, C.M. et al. (2000) Three dimensional climatological distribution of tropospheric
 842 OH: update and evaluation. *J. Geophys. Res.*, **105**, 8931-8980.
- 843 Sriskantharajah, S., et al. (2012) Stable carbon isotope signatures of methane from a Finnish
 844 subarctic wetland. *Tellus B*, 64, 18818, 8p.
- 845 Stein, A. F., Draxler, R. R., Rolph, G. D., Stunder, B. J. B., Cohen, M. D., and Ngan, F. (2015)
 846 NOAA'S HYSPLIT Atmospheric Transport and Dispersion Modeling System, Bulletin of the
 847 American Meteorological Society, 96, 2059-2077, 10.1175/bams-d-14-00110.1.
- 848 Tans, P.P., (1997) A note on isotopic ratios and the global atmospheric methane budget. *Global*
 849 *Biogeochem. Cycles*, 11, 77-81.
- 850 Thompson, R.L. et al. (2015) Methane emissions in east Asia for 2000-2011 estimated using an
 851 estimated Bayesian inversion. *J. Geophys. Res.*, 120, doi:10.1002/2014JD022394.
- 852 Tselioudis, G., Lipat, B.R., Konsta, D., Grise, K.M., and Polvani, L.M., (2016) Midlatitude cloud
 853 shifts, their primary link to the Hadley cell, and their diverse radiative effects. *Geophys. Res.*
 854 *Lett.*, 43, in press.
- 855 Westerman, P. and Ahring, B.K. (1987) Dynamic of methane production, sulfate reduction and
 856 denitrification in a permanently waterlogged alder swamp. *Appl. Env. Microbiol.* 53, 2554-
 857 2559.
- 858 Wolff, E. and Spahni, R. (2007) Methane and nitrous oxide in the ice core record. *Phil. Trans.*
 859 *R. Soc. Lond. A*, 365, 1775-1792
- 860 Worden, J. et al. (2013) El Niño, the 2006 Indonesian peat fires, and the distribution of
 861 atmospheric methane. *Geophysical Research Lett.*, 40, 1-6. doi:10.1002/grl.50937, 2013
- 862 Zazzeri, G., et al. (2016) Carbon isotopic signature of coal-derived methane emissions to
 863 atmosphere: from coalification to alteration. *Atmospheric Chemistry and Physics Discussions*,
 864 doi:10.5194/acp-2016-235
 865